Limited haplotype diversity underlies polygenic trait architecture across 70 years of wheat breeding

Authors: Michael F. Scott[1], Nick Fradgley[2], Alison R. Bentley[2], Thomas Brabbs[3], Fiona Corke[4], Keith A. Gardner[2], Richard Horsnell[2], Phil Howell[2], Olufunmilayo Ladejobi[1], Ian J. Mackay[2†], Richard Mott[1], James Cockram[2]

[1] UCL Genetics Institute, Gower St London WC1E 6BT, United Kingdom

[2] NIAB, 93 Lawrence Weaver Road, Cambridge, CB3 0LE, United Kingdom

[3] Norwich Research Park Innovation Centre, Colney Ln, Norwich NR4 7UZ, United Kingdom

[4] The National Plant Phenomics Centre, Institute of Biological, Rural and Environmental Sciences (IBERS), Aberystwyth University, Gogerddan, Aberystwyth, SY23 3EE, United Kingdom

[†] Current address: SRUC, Peter Wilson Building King's Buildings, W Mains Rd, Edinburgh EH9 3JG, United Kingdom

Corresponding authors:

Richard Mott r.mott@ucl.ac.uk, James Cockram james.cockram@niab.com

These authors contributed equally:

Michael F Scott and Nick Fradgley; Richard Mott and James Cockram

Abstract

Background

Breeding has helped improve bread wheat yield significantly over the last century. Understanding the potential for future crop improvement depends on relating segregating genetic variation to agronomic traits.

Results

We bred NIAB Diverse MAGIC population, comprising over 500 recombinant inbred lines, descended from sixteen bread wheat varieties released between 1935-2004. We sequenced the founders' exomes and promotors by capture. Despite being highly representative of North-West European wheat and capturing 73% of global polymorphism, we found 89% of genes contained no more than three haplotypes. We sequenced each line with 0.3x coverage whole-genome sequencing, and imputed 1.1M high-quality SNPs that were over 99% concordant with array genotypes. Imputation accuracy remained high at coverage as low as 0.076x, with or without the use of founder genomes as reference panels. We created a genotype-phenotype map for 47 traits over two years. We found 136 genome-wide significant associations, concentrated at 42 genetic loci with large and often pleiotropic effects. Outside of these loci most traits are polygenic, as revealed by multi-locus shrinkage modelling.

Conclusions

Historically, wheat breeding has reshuffled a limited palette of haplotypes; continued improvement will require selection at dozens of loci of diminishing effect, as most of the major loci we mapped are known. Breeding to optimise one trait generates correlated trait changes, exemplified by the negative trade-off between yield and protein content, unless

selection and recombination can break critical unfavourable trait-trait associations. Finally, low coverage whole genome sequencing of bread wheat populations is an economical and accurate genotyping strategy.

Introduction

Bread wheat (*Triticum aestivum* L.) production is a critical component of worldwide food security. Demand for wheat is predicted to increase by 60% between 2014 and 2050[1], by which time the human population will have reached 9 billion. Breeding will be a key component of meeting this demand sustainably[2]. Over the past century, genetic gains have been responsible for between one third and two thirds of yield improvements in European wheats, amounting to a 12-120kg increase in yield (~1%) per hectare per year[3–6].

Genomic data is expected to accelerate the rate of genetic gain in wheat[7,8]. Surveys of global standing genetic variation include, for example, whole genome resequencing (WGS) of 93 accessions[9], exome capture for 870 accessions[10], genotyping by sequencing (~16k markers) for ~17k breeding programme lines[11], and genotyping array data for collections of 804[12] and 4,500[13] accessions (~15k and ~113k markers, respectively). Bread wheat's large genome size (17Gb) inflates the cost of collecting sequencing data and its hexaploidy reduces the accuracy and cross-population consistency of genotyping array data[12]. The potential for genotyping by low-coverage WGS in polyploid wheat has yet to be established.

To aid genetic gain through breeding, it is crucial to link genetic data with phenotypic information and thereby reveal genotype-phenotype associations[11,14]. Previous

genotypic/phenotypic datasets include five traits measured in two years for 870 global accessions with exome capture data[10], and 12 traits measured in two years, six locations, and three cropping intensities for 191 German varieties with genotyping array data (~9k markers)[15]. Genotype-trait and trait-trait associations may be confounded by population structure or hidden by low allele frequencies in studies of existing varieties or breeding lines. These problems can be controlled in experimental populations produced by crossing. However, mapping resolution and overall genetic diversity are typically low in experimental populations. Multiparent Advanced Generation Intercross (MAGIC) populations are designed to address these issues by accumulating recombination events through generations of intercrossing and capturing diversity across multiple founders[16–18].

In this study we undertook a systematic approach to these challenges. We bred a new multi-parental population, the 'NIAB DIVERSE MAGIC' population (hereafter 'NDM') through hundreds of structured inter-crosses between sixteen diverse founders. Our multi-funnel crossing design creates a greater number and more uniform genome-wide distribution of recombinant haplotypes than alternative multiparent populations[19] and the relatively large number of diverse founders samples more genetic variation. We sampled founders released between 1935-2004, aiming to determine the genetic basis for historical changes in agronomic traits and the potential for future improvement from within the existing pool of variants. We used a cost-effective genotyping strategy by low-coverage WGS, accurately imputing over 1M SNPs in over 500 recombinant inbred lines. We measured 47 phenotypes in the population, of which 25 were assessed across two growing seasons. The power of NDM comes from the combination of carefully designed germplasm and dense genotypic and phenotypic information, all of which we make publicly available.

We address the following questions. First, what genetic variation exists among the exomes of the NDM founders, how does it reflect global wheat diversity, and specifically how many distinct haplotypes typically segregate at each locus? Second, how does this variation underlie agronomic traits, as revealed through genetic mapping and genomic prediction? And third, what do these models imply about the future potential for phenotypic change and to what extent should we expect selection to cause correlated trait changes due to the sharing of causal genetic variants between traits.

Results

NIAB DIVERSE MAGIC Founders

The 16 founders were selected from a panel of 94 historical varieties released in the UK over a ~70 year period (and originating from the UK, France, Denmark, Sweden and the Netherlands, Supplementary Table 1) using 546 Diversity Array Technology (DArT) and 61 Single Sequence Repeat (SSR) markers[20]. We sequenced 15 founders after enrichment for (a) genic regions and (b) putative promoters using a capture probe-set[21] at average coverage of 22.94x of the targets (Supplementary Table 1). The remaining founder, Holdfast, was sequenced by WGS, but to ensure consistency across founders, we restricted our attention to the capture targets, for which coverage in Holdfast was 15.8x. We sequenced using Illumina 150bp paired-end reads whose combined length often included sequence differences between homeologous loci on the A, B and D subgenomes of hexaploid wheat, thereby resolving otherwise ambiguous alignments. Furthermore, we only used high quality alignments (mapQ>30) for coverage calculations and variant calling, and subsequently

116 excluded variant sites with missing or heterozygous calls in any founder (e.g. from
117 homeologous variation and misalignment). After quality control, we called 1.13M high-quality
118 single nucleotide polymorphisms (SNPs) across the 110,790 promoter-gene pairs targeted by
119 the capture probes (557Mb in total), summarised in Supplementary Figure 1. Only 97,727
120 SNPs (8.7%) were on the D subgenome and almost half (17,289/35,021, 49.4%) of the
121 promoter-gene pairs on the D subgenome had no SNPs passing quality control, compared to
122 26.6% (9,656/36,302) and 21.7% (8,012/36,738) on the A and B subgenomes, respectively. A
123 comparative lack of diversity is expected on the D subgenome as it was acquired in the most
124 recent allo-polyploidisation event[22].
125
126 We placed the 16 founders in the context of global wheat diversity by analysing 113,457
127 genotyping array sites that vary among 4,506 diverse global wheat accessions[13], of which
128 50,335 sites were callable across all founders. We classified global wheats into nested subsets
129 representing the UK only (n=154), North-West (NW) Europe (n=1,343), Europe (n=2,331), and
130 Global (n=4,506), to understand how allele frequencies across subsets relate to our founders
131 (Figure 1). Most Global common variants are polymorphic in the founders whereas rare alleles
132 are more likely to be fixed in the founders, particularly those scarce in NW Europe and the
133 UK. For example, 79.7% of those SNPs polymorphic within the UK subset (which includes
134 landraces) also segregate among the founders, falling to 73.4% Global sites across all 4,506
135 accessions. We next asked whether we could have selected 16 founders that more
136 comprehensively sampled the variation space. We simulated selections from the same nested
137 subsets and compared the distribution of the fraction of segregating sites with that in the
138 actual NDM founders, and found the latter capture more diversity than an average selection
139 of UK wheats, about average diversity for NW European wheats, but less than average for

wider European and Global sets (Figure 1). As the Global dataset is highly diverse, with modern varieties (released 1960-2009, n=2,294), landraces (1800-1959, n=965), and uncategorised/landrace germplasm (n=1,247), we conclude that NDM is representative of NW European wheat germplasm.

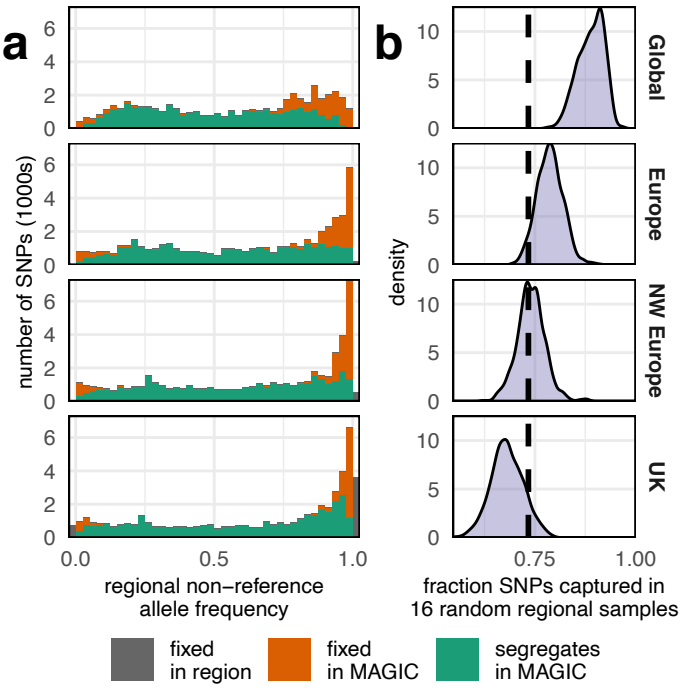

***Figure** 1 The NDM population is representative of NW European wheat. (a) SNPs segregating (green) or fixed (orange) in NDM at 50,335 sites in 4,506 global wheats, grouped into 'Global', 'European', 'North-West European' and 'UK' nested subpopulations and binned by the allele frequency in these subpopulations. (b) The fraction of sites that are polymorphic in 16 randomly chosen wheats from each subpopulation based on 1000 random replications. The dashed vertical black line at x=0.734 is the fraction of SNPs segregating among NDM founders.*

We next estimated the haplotypic diversity in the founders at the 1.13M sites. First, we clustered the founders by their haplotypic similarity at the 73,982/110,790 (66.7%) promoter-gene loci with at least two haplotypes. Assuming that founders carry the same haplotype when their genotypic similarity exceeds 95%, 38,535 loci (52% of loci with variants) had only two haplotypes, 61,438 loci (83%) had at most three haplotypes, and 70,602 loci (95%) had four haplotypes at most (Figure 2b). Second, we estimated haplotype diversity by a dynamic programming algorithm that adjusted locus/block boundaries (Figure 2c, Supplementary Figure 2) to minimise the number of distinct haplotypes within a locus, while balancing

159 transitions between calling identical versus non-identical haplotypes. Over a wide range of
160 parameters, the average number of haplotypes present at any locus rarely exceeded two
161 (Supplementary Figure 2: 81.2% of 1.13M sites inferred to have just two haplotypes). This
162 analysis found slightly fewer haplotypes than the gene-based analysis because it can infer one
163 haplotype (4.1% of sites) when nearby variation is inconsistent, and split genes with high
164 haplotypic diversity into multiple blocks.
165
166 For comparison, the 19 natural accessions that founded the *Arabidopsis thaliana* MAGIC[23]
167 display much greater haplotypic polymorphism[24]. In *A. thaliana*, genic haplotypes were
168 determined at the level of protein sequence similarity (>95% similarity within
169 haplotypes)[24]. On average there were 4.8 protein haplotypes per gene and 7,263/13,919
170 (52.2%) of genes with two (n=4,825) or three (n=2,438) haplotypes (excluding genes with no
171 variation). Our estimates for the NDM founders are 2.7 haplotypes per gene and 83% of
172 variable genes having at most three haplotypes. Protein-level differences are lower than DNA
173 level differences making this comparison conservative, and thus the true difference is even
174 greater.
175
176 ## *The NIAB DIVERSE MAGIC Population*
177 We developed a total of 596 Recombinant Inbred Lines (RILs), each descended from all 16
178 founders via a crossing funnel (Figure 2a). After 6 generations of inbreeding, all 596 RILs were
179 initially genotyped using the Axiom 35k wheat breeders' SNP genotyping array[12]. We called
180 SNPs at 20,688 sites, of which 5,747 overlapped with the 1.13M SNP calls made in the
181 founders. These overlapping sites suggested that only 59.8% of genotyping array probes could
182 have been unambiguously placed using BLASTn[25], underlining the difficulty of using short

183 probes in polyploids (Supplementary Table 2). We used the overlapping sites as a truth
184 genotype set to find sample misidentifications and estimate the accuracy of sequence-based
185 genotyping in the RILs.

186

187 We excluded 46 RILs excessively similar (>92%) to other RILs, indicating possible errors during
188 population development. We sequenced the remaining 550 RILs after 7 generations of
189 inbreeding by low coverage WGS (mean 0.304X) and called variants at the 1.13M founder SNP
190 sites using sequence alignments. A further 46 RILs were excluded as their genotypic
191 concordance with the initial 35k array data was below 95%, leaving 504 RILs in 141 families
192 (RILs in the same 'family' are derived from the same 16-way cross), from which we based our
193 main analyses.

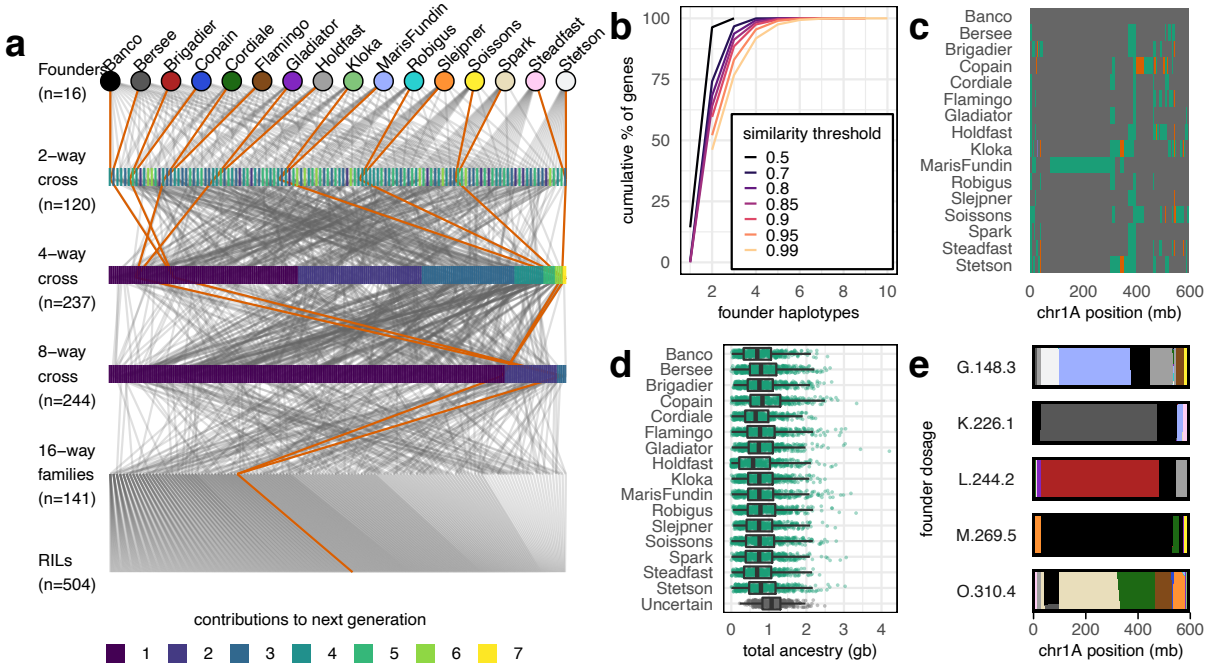

194

195 ***Figure 2*** *NDM population design and haplotypic diversity. (a) Pedigree showing the construction of 504*
196 *Recombinant Inbred Lines (RILs). One exemplar pedigree is highlighted to show how all 16 founders are*
197 *intercrossed into each RIL. (b) Founder haplotype groups at 73,982 promoter-gene loci with SNP variation, where*
198 *founders with the same haplotype have genotypic similarity fractions that exceed the corresponding threshold.*
199 *(c) Pairwise similarity/dissimilarity between founders on chromosome 1A, determined using a dynamic*
200 *programming algorithm to infer founder similarity and breakpoint position. Founders that are inferred to have*
201 *similar haplotypes for each region are the same colour. (d) The total length of genomic blocks in NDM lines*
202 *inferred to come from each founder; uncertain ancestry blocks have a maximum founder dosage of <90%. (e)*

Inferred founder dosage and ancestry mosaics across chromosome 1A for five example RILs, with founders coloured as in (a).

We imputed RIL genotypes using STITCH[26] by inferring the founder haplotype carried by each line at each location. Figure 2c shows the haplotypic similarity among founders on chromosome 1A, indicating that a small number of haplotypes have been heavily recombined during the 69 years of breeding history that separates the founders. Most recombination is located towards the distal ends of the chromosomes, as expected[27]. Only limited further recombination occurs during MAGIC population construction and the haplotype blocks inherited from each founder are relatively long (Supplementary Figure 2) and therefore distinguishable from one another. Thus, it was necessary to assume 16 unique haplotypes were segregating to obtain the highest imputation accuracy (Supplementary Figure 2). Founder haplotypes could be confidently assigned (i.e. with >90% dosage from a single founder) at over 92.2% of sites (Figure 2d). These haplotype assignments implied that an average of 4.8-13.7 recombination events occurred per RIL per chromosome (mean 8.7 sd 2), giving an average of 183 (sd 36.3) recombination events per RIL in total. Consistent with estimated genetic map lengths of 35-37.4M[12,28], 4.9-5.2 recombination events were observed per Morgan, in line with the predicted ~5-fold increase in 16-parent MAGIC populations compared to two-way crosses[29]. Example founder haplotype mosaics across chromosome 1A are shown in Figure 2e.

The fraction of sites called directly (i.e. without imputation) for 501 RILs varied between 20.9-42.7% (mean 27.8% sd 3.4%), as expected for 0.3x-coverage sequence data. A further three RILs were sequenced to higher depth (2.7x, 4.0x, and 4.3x) and had call rates of 79.9%, 90.0%, and 93.0%, respectively (Figure 3a). After imputation, 94.2% of the 1.13M SNPs (i.e. 1.07M) were called across all 504 RILs and the effective call rate of imputed sites was 99.6%, with

5.8% of the SNP sites inaccessible or removed by quality control: 0.93% of sites are on the "Un" chromosome in the wheat reference (excluded from imputation), 1.36% were removed by imputation QC (info score <0.4) and 3.52% had imputed minor allele frequencies below 2.5% and/or missingness above 90%. Figure 3b shows that the concordance between array and imputed genotypes (AI) and between array and directly called genotypes (AD) are strongly correlated, suggesting that instances of poorer concordance are unlikely to be caused by imputation. Overall, imputation marginally improved accuracy versus direct calls (mean AI 99.1% versus mean AD 99.0%) but increased the call rate three-fold. Downsampling read coverage showed the founder haplotype space and recombination mosaics could be accurately inferred from coverage as low as 0.076x per sample (Figure 3c); above this level imputation accuracy was independent of whether founder haplotypes were included as a reference panel (mean AI 98.7%) or ignored (mean AI 98.5%).

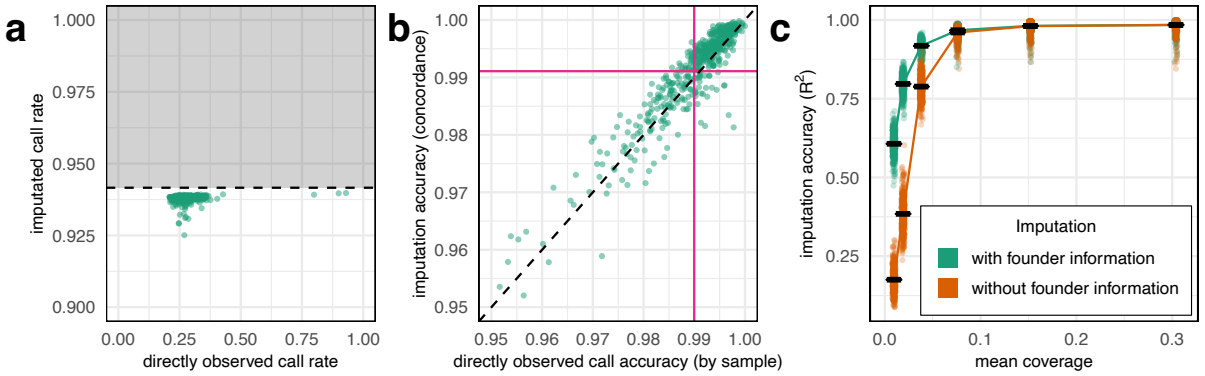

Figure 3 *Call rate and accuracy of genotypes after imputation and after downsampling. (a) Imputed call rate (y-axis) vs direct call rate (x-axis. Only 28.1% of the 1,131,251 SNP sites can be genotyped directly from the low coverage sequence data, whereas 93.8% of sites had genotypes after imputation. 5.8% of sites (grey region and horizontal dashed line in a) were removed by quality control filters after imputation or on the unimputed 'Un' chromosome (0.93%). (b,c) Accuracy as evaluated at 5,747 sites that overlap with the Axiom 35k array. (c) Imputation before/after downsampling was performed with (green) and without (orange) using the genotypes of the founders as a reference panel.*

Introgressions and Segregation Bias

Several recent studies have used genomic data (e.g., SNP density[9]) to study the introgression of genetic material into hexaploid bread wheat from the secondary and tertiary gene pool[9,10,30]. We examined evidence for introgressions in previously reported locations[9,31–33] using founder coverage and non-reference allele frequency. Because we developed RILs, we were also able to examine segregation bias, which often accompanies wheat introgressions[34,35]. We found evidence for at least six introgressions covering ~1.1Gb segregating in the population, five of which showed segregation bias (Supplementary Table 3).

Phenotypic Characterisation and QTL Mapping

We measured 47 phenotypes in replicated field trials over two years (Table 1, Supplementary Tables 4, 5, and 6), including the 10 time points at which Green Leaf Area (GLA) was measured. Of these, 25 phenotypes were collected in both years and two were also measured in smaller 1x1m nursery plots (Yellow Rust infection, YR, and Juvenile Growth Habit, JGH) to give a total of 73 phenotypic measurements. Phenotype distributions are shown in Supplementary Figure 3, showing that some RILs have more extreme phenotypes than any founder (transgressive segregation) for almost all phenotypes (RIL maximum ≥ founder maximum for 61/73 phenotypes and RIL minimum ≤ founder minimum for 68/73 phenotypes). All phenotypes have significant ($p<0.05$, Pearson's correlation test) correlations with at least one other phenotype (Supplementary Figure 4).

Table 1 Phenotypes collected

ABBREVIATION	TRAIT	ABBREVIATION	TRAIT
BIS	Basal infertile spikelets	GS55	Ear emergence date
EL	Ear length	GS65	Anthesis date
ETA	Ear taper	GW	Grain width
ETS	Ear tip sterility	GY	Yield

EW	Ear weight	HEB	Height to ear base
FLA	Flag leaf angle	HET	Height to ear tip
FLED	Flag leaf to ear distance	HFLB	Height to flag leaf base
FLF	Flag leaf floppiness	JGH	Juvenile growth habit
FLL	Flag leaf length	LOD	Lodging
FLS	Flag leaf senescence	PHS	Pre-harvest sprouting
FLW	Flag leaf width	PIG	General pigmentation
GA	Grain area	SH	Spring habit
GL	Grain length	SPIG	Stem pigmentation
GLA#	Green leaf area (10 time points, Nov–Mar)	SW	Specific weight
GLAU	Glaucousity	TGW	Thousand grain weight
GPC	Grain protein content	TIS	Tip infertile spikelets
GR	Germination rate	TS	Total spikelets
GS39	Flag leaf emergence date	YR	Yellow rust infection

From the 1.07M imputed SNPs, we selected a subset of 55,067 pruned by linkage disequilibrium (LD). Using genome-wide association scans (GWAS) on both SNP and founder haplotype data, we mapped 136 Quantitative Trait Loci (QTLs) across the 73 phenotype/year combinations that were genome-wide significant at the 5% level. Many QTLs overlapped for different phenotypes, clustering into 42 distinct genome locations. For 25 phenotypes that were measured in both years, we found 48 QTLs in year 1 and 49 QTLs in year 2, of which 28 were mapped to the same location and were genome-wide significant in both years. For example, in replicated trials lacking fungicide treatment we mapped yellow rust (*Puccinia striiformis*) susceptibility to four QTLs in year 2 (on chromosomes 2A[31,36], 2B[37], 3B, and 6A), of which three were also mapped in year 1 (2A, 3B, and 6A); only one (6A) was also mapped in trials treated with fungicide. 126/136 QTLs at 40/42 genomic locations were mapped using SNP-based associations, whereas 87/136 QTLs at 30/42 genomic locations were mapped using haplotype-based association tests. That is, 10 QTLs and two genomic locations were only identified from haplotype-based association whereas 49 QTLs and 12 genomic locations were only identified from SNP-based association. This is consistent with the limited gene-level haplotypic diversity observed among the founders.

289 Figure 4b summarises the 40 loci with genome-wide significant SNP-based associations. We
290 were able to assign 21 of these, including most of those with the strongest effects, to
291 previously reported QTLs. In 11 high confidence cases, candidate genes have been reported
292 and/or validated experimentally. In other cases, QTLs contained homeologs or paralogs of
293 these high confidence candidates, or previous studies had reported associations to a genetic
294 map using marker data, but not firmly anchored these locations on the reference genome
295 assembly (low confidence co-localisation, n=10). We checked six high confidence candidate
296 loci with annotated reference genome locations (*RHT-1*[38], *RHT-2*[39], *WAPO-A1*[40], *ALI-*
297 *1*[41]*, TaMyb10-B1*[42], *Yr7*/*Yr5*/*YrSP*[37], *PPD-D1*[43]), all of which were within our mapping
298 intervals. We created a genotype-phenotype map for community use by placing all QTLs on
299 the physical map (Supplementary Table 7) to a median interval of 9.2Mb.
300
301 Most loci with strong effect co-localise with previously reported QTLs. Some large effects are
302 commonly associated with adaptation of the founders to the geographic and temporal range
303 they sample. For example, the early flowering allele at the photoperiod locus *PPD-D1* carried
304 by the founder Soissons is favoured in southern Europe to avoid the summer drought[44].
305 The modern semi-dwarfing alleles at *RHT-B1* or *RHT-D1* that have been favoured globally
306 since the Green Revolution[45] are absent from founders Banco, Bersee, Copain, Flamingo,
307 Holdfast, Kloka, Spark, Steadfast and Stetson.
308
309 To examine the pleiotropic effects of the relatively few genome-wide significant QTLs, we
310 took the most strongly associated SNP at each locus and then tested for associations with all
311 other phenotypes, requiring a lower threshold for evidence of association ($p<0.05$) than was
312 initially used to establish genome-wide significance. The results are visualised in Figure 4d,

313 which shows that loci significant for one phenotype are also common to other phenotypes,
314 consistent with extensive pleiotropy and the shared genetic control of correlated phenotypes.
315

316 ## *Gene Deletions*

317 Our analysis of SNP variation ignored sites that could not be called reliably in all 16 founders,
318 possibly due to whole-gene deletions relative to the reference genome. We obtained no
319 coverage from at least one founder at 8,019 (7.2%) of genic regions and 1,095 (1.1%) of
320 promoter-gene pairs, suggesting possible structural variations (Supplementary Figure 1).
321 Based on the deviation in gene coverage from that expected given the mean coverage for the
322 founder, we computed a quantitative gene deletion score (GDS) for each gene and founder
323 and imputed the scores into the RILs using the founder ancestry mosaics. We tested the
324 association between each GDS and each phenotype in order to identify potential causal
325 deletions. Across 27/73 phenotypes we found 30 GDS associations with p-values $<10^{-6}$
326 (Supplementary Table 8). Significant associations almost always occurred within QTLs
327 previously mapped by SNP association, so this analysis only identified candidate genes with
328 deletion status consistent with the pattern of action across the founders of a QTL. Of these,
329 at 10 loci the peak GDS logP association was at least 90% of the peak SNP logP. Thus most
330 QTLs are not likely to be caused by gene deletions. However, the GDS is based on empirical
331 read coverage, and so is likely to be affected by stochastic experimental variations hence it is
332 possible that the association at a true causal GDS might appear weaker than that of a tagging
333 SNP. A further caveat is that deletions are always inferred relative to the reference genome
334 of Chinese Spring, such that insertions or functional genes missing from the reference genome
335 annotation will not be captured.
336

Genomic Prediction

We next performed phenotypic prediction all 55,067 tagging SNPs, to predict the potential for genetic improvement within the NDM. We trained genomic prediction models using three shrinkage methods: ridge regression (RR), least absolute shrinkage and selection operator (LASSO) and Elastic Nets (EN), using 50-fold cross-validation with randomly-selected training sets comprising 90% of RILs and test sets of the remaining 10%. LASSO and EN had almost identical prediction accuracies but EN included on average 26% more SNPs than LASSO (Supplementary Figure 5). Accordingly, we only report the LASSO results. LASSO prediction accuracies for all traits are shown in Figure 5b, alongside the proportion of heritable variation explained by QTLs (Figure 5a). Across traits, LASSO had higher average prediction accuracy than RR (Figure 5c), particularly for phenotypes where a larger fraction of variation can be explained by genome-wide significant QTLs (Figure 5d), as expected for a model selection method. LASSO prediction accuracies (correlation coefficients) varied from 0.13-1 (mean 0.43) across phenotypes, using models with 1-465 SNPs (mean 155 SNPs). The number of SNPs in the LASSO model is higher for phenotypes where the overall heritability estimate greatly exceeds the fraction of variation that can be explained by genome-wide significant QTLs (Figure 5e).

Out-of-sample test set prediction confirms that polygenic LASSO SNPs have predictive power and are therefore likely to be tagging genetic variants affecting phenotypic variation. Most phenotypes are polygenic; their prediction models exhibited a mixture of a few large effect and many smaller effect loci. A typical example (for height) of the 193 non-zero LASSO SNP effects is shown in Figure 4c. In contrast, the Mendelian AWN phenotype is fully explained and predicted using a single genome-wide significant QTL.

The reduced accuracy of RR compared to the LASSO is expected in the absence of significant population structure. There will be reduced variation in kinship among RILs compared to the wider germplasm from which the founders are usually selected. Much of the prediction accuracy of RR results from exploiting kinship rather than from tagging causative variants[46] so there is less opportunity for high prediction accuracy in MAGIC populations. In these circumstances, a feature selection method such as the LASSO can more accurately identify and tag haplotypes contributing to trait variation and give greater prediction accuracies. The LASSO also accurately predicts traits determined predominantly by a few QTL of large effects, in which circumstances RR performs poorly (Figure 5d). The LASSO is therefore better for genomic prediction in MAGIC.

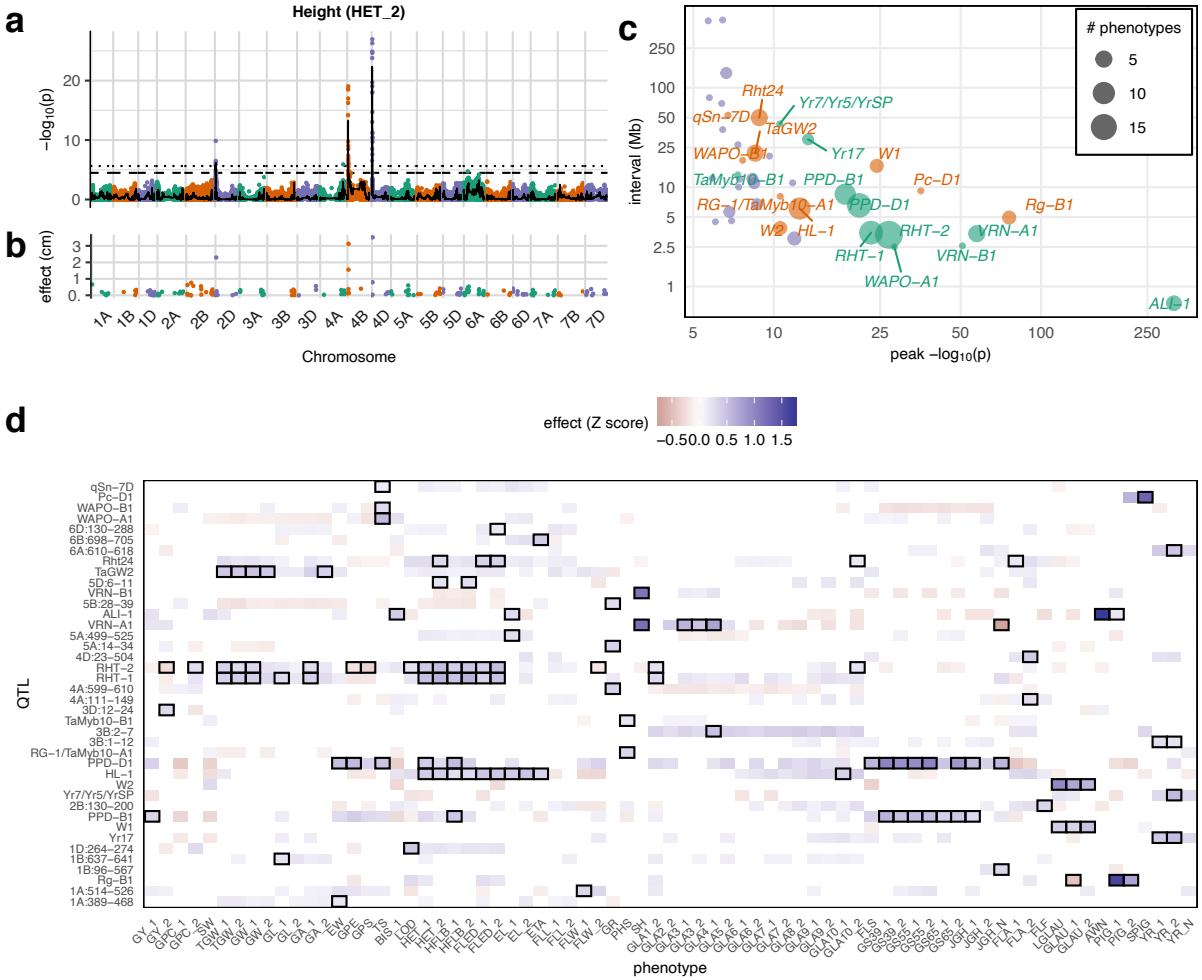

Figure 4 *Genotype-phenotype associations. (a) Exemplar Manhattan plot of the genome-wide -log$_{10}$ p values of association (logP) between the height to ear tip phenotype from year 2 (HET_2) and 55,067 LD-pruned SNP dosages (dots) or founder haplotype dosages (line). The horizontal lines show the 5% genome-wide significance thresholds for SNPs (dotted) and haplotypes (dashed). (b) The 193 non-zero estimated LASSO SNP effects for HET_2. (c) The 40 genomic locations where genome-wide significant SNP associations were found for at least one phenotype, classified by effect size (logP; x-axis) and genomic interval width (Mb; y-axis). Each circle represents one locus, and its size shows the number overlapping QTLs; the smallest interval width and p value is shown where there are multiple overlapping phenotype associations. Labels indicate QTLs that colocalise with previously described QTLs or candidate genes; green indicates high-confidence colocalization (n=11) and purple low-confidence colocalization (n=10). (d) Pleiotropy across 40 loci: those loci without names are labelled by chromosome and position in Mb) and 73 phenotypes. Shades indicates the significant (p<0.05) locus phenotypic effects expressed as the number of standard deviations (Z-score). Genome-wide significant QTLs are highlighted with boxes.*

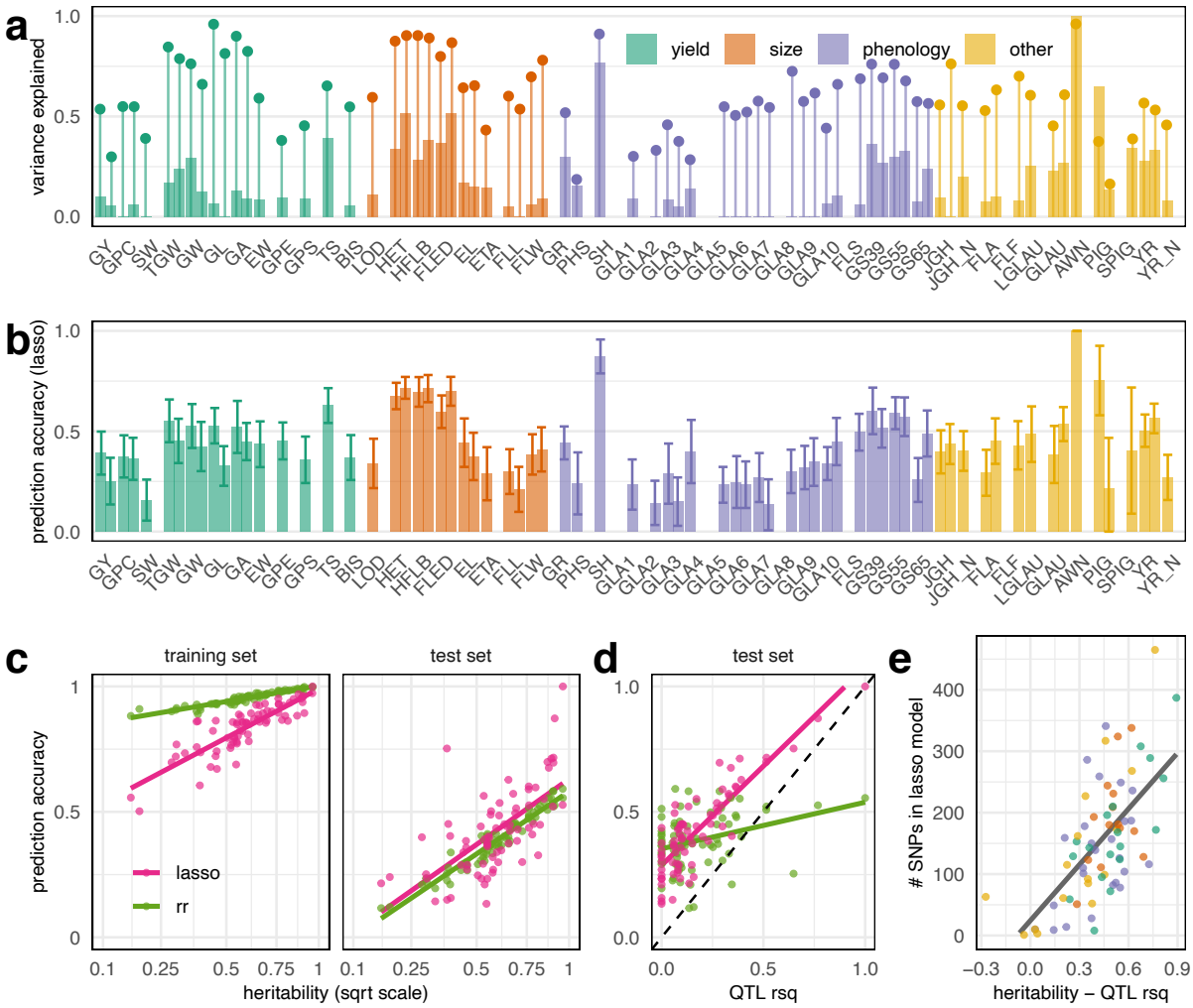

Figure 5 *Genetic architectures of 73 trait/year combinations (47 distinct traits) as revealed by QTL mapping and genomic prediction. (a) Phenotypic variation explained by all genome-wide significant QTLs (thick bars) and by the full SNP-based genetic relationship matrix (heritability, thin bars and dots). Phenotypes measured in year 1 and year 2 are paired, shifted to the left and right, respectively. (b) LASSO prediction accuracy (correlation coefficients) across 50-fold cross validation; error bars show sds. (c) Prediction accuracy correlations (y-axis) and sqrt(heritability) (x-axis) and in the test and training sets under ridge regression (rr) and LASSO genomic prediction models. Prediction into the test set is generally higher with LASSO, especially for traits where more variation is explained by genome-wide significant QTLs (d). (e) LASSO models usually include more SNPs when more heritable variation is unaccounted by genome-wide significant QTLs (x-axis is difference between heritability and QTL R^2).*

We used these genomic prediction models to explore the potential for selection in a much larger simulated population of 20,160 MAGIC RILs, 40 times larger than the real population. These were created by permuting the founder identities in the founder genome mosaics inferred in the real RILs, preserving linkage through the genetic map. Phenotypes were predicted for the test set of real RILs (10% of all lines) and in the simulated RILs for all 50 prediction models (training/test set jackknife resamples). Figure 6a shows, for two example

phenotypes, that the distribution of predicted phenotypes is almost identical in the real (test set) and simulated RILs. As expected, the most extreme predicted values (maximum and minimum) in the simulated RILs exceed than those in the real dataset because novel allelic combinations are generated in the larger simulated population. However, the average improvement in extrema between the test set and simulated phenotype predictions is only -0.5 (for the minimum) and +0.68 standard deviations (for the maximum). This is in line with extreme-value distribution theory and shows that blind-breeding a very large population in the hope of generating novel combinations of beneficial alleles is inefficient.

Next, we predicted the theoretical extreme phenotypic values that it is possible to create from segregating variation if unlimited recombination were possible. That is, we computed the phenotypic prediction in an imaginary line that carries all the alleles predicted to increase/decrease each phenotype. For this exercise, we trained the prediction models on the full set of 504 RILs so they differ slightly from those used to predict phenotypes in the test set. In the test set and simulated RILs, the predicted phenotypic extremes generally reflect the population size, which determines the probability that a single line happens to sample many alleles with positive/negative effects. However, Figure 6b shows that the theoretical maximum/minimum phenotypic prediction is linearly related to the complexity of the LASSO model (i.e. the number of non-zero SNP coefficients in the model). This suggests that hundreds of loci would need to be selected over multiple generations to generate any large phenotypic shifts, in line with the decades of breeding that has been required to produce genetic gain.

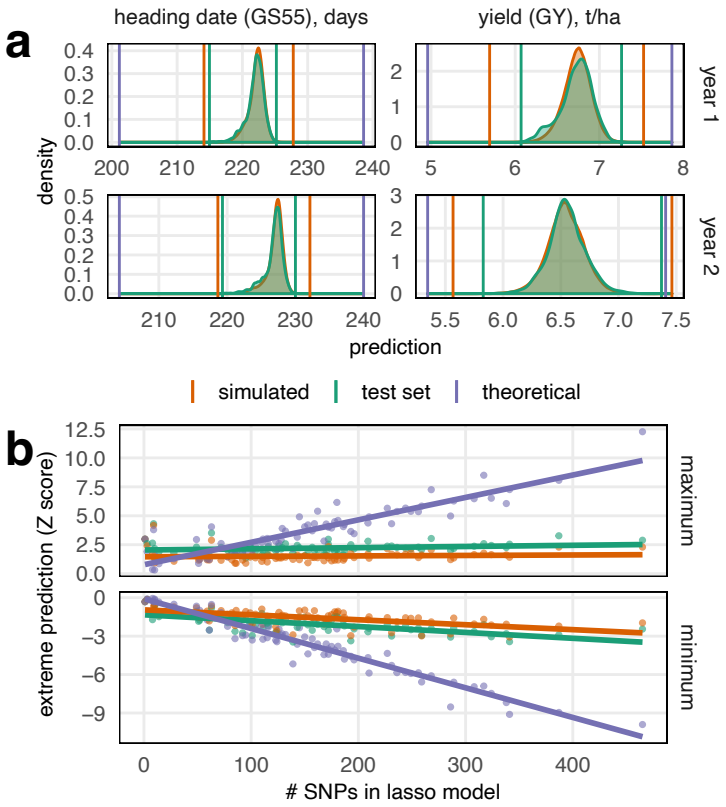

Figure 6 *Predicted potential for phenotypic change. (a) We predicted the phenotypes of real MAGIC recombinant inbred lines, RILs (green distribution), and a large population of 20,160 simulated MAGIC RILs (orange distribution). These distributions largely overlap but more combinations are made in the simulated dataset such the the extreme values are more extreme. Nevertheless, the highest/lowest phenotypic prediction in the simulated population of 20,000 is generally only ~0.5 standard deviations higher/lower than the trait predictions in the real dataset of 504 lines. Upper graphs: predictions based on year 1 phenotype, lower graphs predictions based on year 2 phenotype (b). We also estimated the extemes of the phenotype predictions that are possible given the full lasso genomic prediction models (purple line in a). Large deviations from the current population mean are predicted to be possible but only through the fixation of a large number of loci, with less potential for change predicted at less-highly polygenic traits.*

For essentially all crops where yield and yield quality are high priority traits, a trade-off is evident between these two phenotypes and this is recognised as a longstanding problem in wheat. Thus, identifying opportunities to break this trade-off is important[47,48]. We estimate that yield has increased by 0.021 t ha^{-1} $year^{-1}$ based on a regression of average yield on founder release year ($p=0.006$, $n=16$, $R^2=0.43$). The highest yields measured in founders and RILs exceeds the maximum predicted yield from the genomic prediction models (Figure 6) due to shrinkage in estimating SNP effects. However, high grain yield (GY) is correlated with low grain protein content (GPC) among the founders (Pearson's correlation coefficient -0.94,

444 p<0.001, n=16), Figure 7. Founder genetic material is reshuffled without selection in the RILs,
445 but the GY-GPC relationship continues (correlation -0.77, p<0.001, n=504), suggesting some
446 pleiotropy in the underlying genetic effects. To investigate the segregating genetic variation
447 that may be available to break this trade-off, we analysed the deviation from the trend (PYD:
448 distance from symmetrical Thiel-Sen regression between GPC and GY, after Z-score
449 normalisation). The heritability for PYD was 0.41 in year one and 0.25 in year two and could
450 be predicted with accuracy 0.26 (sd 0.11) in year one and 0.13 (sd 0.11) in year two. These
451 estimates are lower than those for GY and GPC analysed separately (GY heritability 0.54 and
452 0.30, prediction accuracy 0.39 and 0.25; GPC heritability 0.55 and 0.55, prediction accuracy
453 0.375 and 0.36, Figure 5. PYD of the founders did not correlate with release date, but these
454 results suggest modest potential to break the yield-protein trade off, requiring strong and
455 targeted breeding effort[47,48].
456

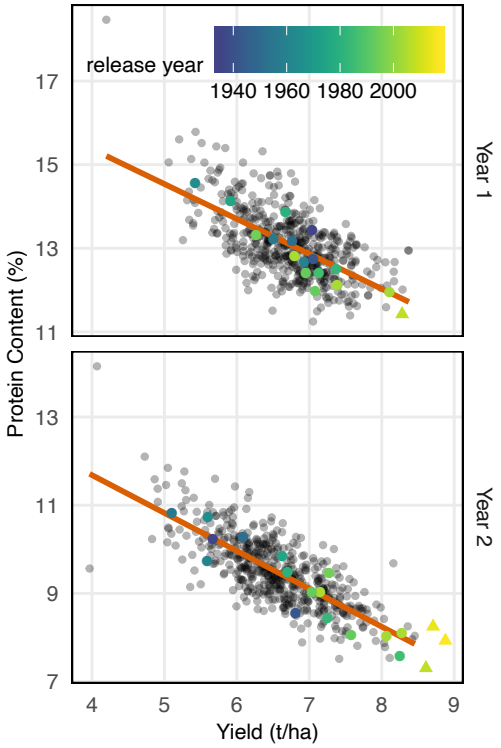

Figure 7 *Negative trade-off across two years between grain yield (GY; x-axis) and grain protein content (GPC; y-axis) in 504 NIAB DIVERSE MAGIC RILs, 16 founders, and 3 more recently developed varieties (triangles, only one measured in year 1).*

Discussion

We report five main findings. First, imputation from low coverage WGS is a cost-effective and straightforward genotyping strategy for crops, at least in multiparental populations. Despite its large, repetitive and hexaploid genome, wheat genotypes can be reliably imputed from WGS with average per-sample coverage in the range of 0.075x-0.3x and without the use of reference panels[26]. Thus there is no absolute requirement to even know the identities of, let alone sequence, the population founders, although this may be desirable for other purposes such as pan-genome assembly and re-annotation[18,49]. In this study, we were able to impute genotypes and founder haplotypes at >1M SNP sites in >500 NDM RILs, which proved ample for genetic mapping and genomic prediction.

Second, based on SNPs called from exome capture, no more than three haplotypes segregate at most genes in commercial NW European bread wheats released since 1935. There appears to be little or no variation at about a quarter of genes on the A and B subgenomes, and at about half on the D subgenome. Complete re-assembly and re-annotation of the 16 founders of the NDM would yield more complete insights into the extent and impact of coding variation. Limits on haplotypic variation are probably the result of historical selection and population bottlenecks that reduced the effective population size before the onset of intensive breeding programmes[12,50], as well as the close relatedness among breeding materials in more recent wheat pedigrees[51]. However, it appears that the low overall level of genetic diversity has not been further reduced during the 20th Century[52,53].

Third, as a consequence, most QTLs are accounted for by bi-allelic SNPs rather than haplotype differences. For comparison, about 40% of QTLs identified in a multi-founder population of rats were attributed to multi-allelic/haplotypic effects[54]. Furthermore, most genome-wide significant QTLs had pleiotropic effects. Extensive pleiotropy suggests that naïve selection on one phenotype is likely to induce correlated responses in other phenotypes. In particular, we found improved yields in recent varieties has come at the cost of a decline in protein content (Figure 7; increasing yield by one t/ha reduces protein content by about 1%). Despite reshuffling haplotypes without selection, this trade-off continues in the NDM, which indicates directed selection would be required to break the yield-quality trade-off, potentially creating varieties with improved nitrogen use efficiency[55,56].

Fourth, across 47 phenotypes, we found a wide range of underlying genetic architectures. For traits such as awns, pigmentation, spring habit and yellow rust resistance, almost all of the

heritable phenotypic variance could be explained by one to four genome-wide significant QTLs (Figure 5). In other cases, a few loci with large phenotypic effects were accompanied by dozens of loci with smaller effects on traits such as flowering time and height (Figure 4a). The loci with very large effects have mostly been reported before (Figure 4b) because we recapitulate key historical steps such as the introduction of photoperiod sensitive and semi-dwarfing alleles from Japan[44,45]. Traits such as yield were polygenic with the majority of heritable variation coming from many loci of smaller effect (Figure 5).

Fifth, our genomic prediction models suggest that hundreds of loci will need to be selected and fixed to achieve large phenotypic changes in polygenic traits in the future (Figure 6B). We achieved reasonable prediction accuracy with modest numbers of SNPs; the mean out-of-sample prediction accuracy was 0.43, using on average only 155 SNPs per phenotype, out-performing ridge-regression which considers all markers simultaneously. Other crop and livestock studies have also found very sparse markers can be sufficient for useful genomic prediction[11,57,58]. Here, rather than using low marker densities, we trained models that select a few hundreds of markers from ~55k tagging SNPs. In part, this sparsity is a consequence of the design and construction of MAGIC populations, eliminating rare alleles and creating blocks of markers that can be easily tagged in prediction models[15]. These factors may be responsible for the use of far fewer markers than used to generate polygenic prediction scores in humans[59], where there is a long tail of rare variation and less linkage disequilibrium.

Our results suggest that dramatic genetic improvement over 70 years of breeding has largely been achieved through the fine shuffling of a low number of haplotypes to recombine

polygenic alleles of small effect, combined with the introduction of alien introgressions from wide crosses. The introgression of large genomic segments from related species has most commonly been for sources of resistance to specific diseases[9,33,34]. Breeders now have a choice whether to continue with the same strategy, i.e. selecting from within existing variation and introgressing selected exotic alleles, or to ambitiously expand the pool of available haplotype diversity genomewide.

Methods

NDM Population Creation

The 16 NDM founders were chosen to capture the greatest genetic diversity using PowerMarker genetic analysis software[60]. They were chosen from 94 NW European wheats released in the UK that were genotyped with 546 DArT and 61 SSR markers; the full panel also included 96 US and 50 Australian varieties, which were excluded based on STRUCTURE analysis[61]. The founder selection process was run iteratively with the varieties 'Robigus' and 'Soissons' first fixed to be included to coincide with the founders of the 8-founder NIAB Elite MAGIC population[62]. Then the most frequently selected additional 4, then 9, and 12 varieties were fixed in multiple iterative selection runs and finally the most frequently selected 16 were chosen. Seed for the founding varieties was sourced from the John Innes Centre Germplasm Resource Unit (GRU http://www.jic.ac.uk/germplasm/).

These founders were inter-crossed in a balanced funnel crossing scheme, based on a Latin square field trial design, over four generations to create 16-way crosses with all the founders equally represented in their pedigree. First, all 120 possible 2-way crosses between founders

were made in a half diallel scheme. Two-way plants were then crossed in 60 4-way combinations. Multiple plants from each family were used in crossing from 2-way onwards, in order to maintain maximum founder allelic diversity within the population. 30 crossing combinations were made between 4-way plants to create 8-way crosses, making between five and eight replicate crosses per combination using different plants. These were intercrossed in 15 combinations to create balanced 16-way crosses, with each combination replicated between six and fifteen times using different 8-way plants. This resulted in 174 16-way plants from which one to sixteen inbred lines per 16-way family were made through single seed descent (SSD). 596 RILs were advanced to the F_7 stage when seed for phenotyping was multiplied in 1x1m nursery plots. Supplementary Table 9 gives details the number of plants involved in each cross and Figure 2a shows the pedigree for the 504 RILs used in our main analysis only.

Phenotyping

RILs from the population were phenotyped in field trials over multiple environments near Cambridge, UK. Yield trials were conducted in the growing seasons 2016-2017 and 2017-2018, hereafter year 1 and year 2 (phenotype suffix codes _1 and _2). Information on location, soil type, key dates and inputs for both years are given in Supplementary Table 4. Yield plot dimensions were 2m wide and 4m long and plots were sown at a density aiming to achieve 300 plants m^{-2} . In year 1, 596 lines were included in two replicates, the sixteen founders in four replicates and the commercial control variety 'KWS Santiago' in 24 replicates in a randomised nested block design with 16 main blocks of 80 adjacent plots which comprised each row in the trial and eight sub-blocks of ten plots nested within each main block. In year 2 trials, 596 lines and the 16 founders were included in two and four replicates respectively

but three control varieties ('KWS Santiago', 'Skyfall' and 'Shabras') were all included in four replicates. Plots were again randomised in a nested block design but including additional plots making a larger trial, consisting of 20 main blocks of 115 adjacent plots, which comprised each row, and 23 sub-blocks of five plots nested within each main block.

Disease observation trials (DOTs) were conducted near Cambridge, UK in the same years as the yield trials to assess resistance to crop diseases. These plots consisted of two 1.2m length rows, treated with no fungicide but otherwise standard inputs. Due to local conditions, DOTs were considered to have natural high pressure of yellow rust (*Puccinia striiformis* f.sp. *tritici*). In both years, DOTs included two replicates of 596 RILs, four replicates of the 16 founders and 68 additional replicates of the susceptible founder 'Robigus'. Trial designs included two main blocks of 660 plots, with 11 sub-blocks of 60 plots nested within main blocks. All trial designs for both yield and disease observation trials were made using the package 'blocksdesign' in R. Phenotyping of some traits was also carried out in 1x1m seed nursery plots where lines were not replicated but the founders were in three replicates and randomised across the nurseries (phenotype code _N).

A wide range of traits were phenotyped across the field trials, including traits for crop developmental morphology, phenology, plant stature and canopy architecture, yield and yield components such as spike and grain morphology, disease resistance, pigmentation, plant glaucosity, indications of stress response, lodging, grain protein content and vernalisation requirement. A summary of these traits and abbreviations are presented in Table 1 and details of phenotyping methods are listed in Supplementary Table 5.

590 ## *Trials Analysis*

591 Adjusted phenotype values were calculated as Best Linear Unbiased Estimates (BLUEs) for
592 each trait separately for each trial year using mixed effects models with ASRemL[63].
593 Genotype was considered a fixed effect whilst experimental blocking structure as well as
594 other covariates such as harvesting day, where relevant, were included as random effects.
595 Spatial models including first- and second-order auto-regressive spatial models were also
596 used. Model simplification was carried out where models with all possible combinations of
597 random effect terms and spatial terms for row and column were run and the best fitting
598 model was chosen based on Akiake Index Criteria (AIC). Model residuals were visually checked
599 for normality and equal variance to fitted values distribution. Best Linear Unbiased Estimates
600 (BLUEs) for all phenotypes for the 16 founders and for the 504 RILs used in our main analysis
601 (see below) are provided in Supplementary Table 6. We used symmetrical Thiel-Sen
602 regression (implemented in the 'deming' R package) after phenotype normalisation to
603 characterise the relationship between protein content (GPC) and yield (GY). The Protein-Yield
604 Deviation (PYD) phenotype is calculated as the Euclidian distance from this regression line.
605

606 ## *Genotyping Array Data*

607 All DNA extraction was performed using the Qiagen DNeasy Plant Kit on leaf tissue samples
608 taken from emerging leaves of seedlings. First, genotyping was performed at the Bristol
609 Genomics Facility using the Axiom 35k wheat breeders' array[12]. Initially, two 384-sample
610 plates were genotyped. Seed from the plants used as founders were genotyped on each plate
611 (32 samples) along with extra seed from the original varietal seed stock used (28 samples)
612 and seed from founders propagated to 2017 (16 samples). In addition, 596 RILs were
613 genotyped after 5 generations of selfing (F_6). To account for genotyping failures and to ensure

614 the accuracy of sample labels, 150 RILs were re-genotyped in the F_7 generation along with a
615 further replicate of each founder.
616
617 Genotype calling was performed using the Affymetrix Power Tools (v1.19) and SNPolisher R
618 packages, following the recommended Axiom analysis pipeline. All samples except two-way
619 crosses were given the standard inbreeding penalty, 4, which penalises calling heterozygous
620 genotypes. Four samples failed the 'dish quality control' threshold (0.82) and a further 28
621 samples with call rates were below 97% were excluded. Marker classifications were
622 performed using "ps-classification", and ps-classification-Supplementary" functions with
623 options --species-type polyploid --hom-ro false. All calls were adjusted using the standard
624 0.025 confidence threshold using the Ps_CallAdjust function.
625
626 Samples were compared to one another using the 14,935 markers classified as
627 'PolyHighResolution' only. Overall, 46 RIL pairs were found to be >92% similar (mean 98.5%
628 genotype similarity), where all other comparisons between MAGIC lines were, at most, 84%
629 similar (mean 67.8%). These apparently duplicated genotypes could indicate genotyping,
630 labelling, or propagation errors so only one RIL from each pair was used for sequencing (550
631 RILs). To ensure pedigree accuracy, we chose the RIL in each pair that was genotypically most
632 similar to other RILs derived from the same 16-way cross (i.e. in the same family).
633
634 *Sequencing Data*
635 For whole genome sequencing, DNA was extracted from 550 RILs at the F_7 generation. DNA
636 for RILs that failed quality control were extracted again at the F_8 generation (n=50).
637 Sequencing and library preparation was performed at Novogene, where libraries were

638 generated from 1.0µg DNA per sample using the NEBNext DNA Library Prep Kit. Sequencing
639 was performed on a NovaSeq 6000 instrument (Illumina) to get at least 6Gb of raw sequence
640 data (2x150bp paired end reads) per sample. One founder (Holdfast) was sequenced to 15.8x
641 coverage using the same method.
642
643 The other founders were sequenced after capture using two recently designed probe sets
644 targeting promoter and genic regions, respectively[21]. Capture was performed at the
645 Earlham Institute following the SeqCap EZ Library SR v5.1 protocol (Roche NimbleGen Inc.,
646 Madison, WI, USA) with 1µg of genomic DNA sheared to 300bp[21]. Four captures were
647 performed using 8 samples per set (2x promoter captures and 2x genic captures). Samples for
648 the founder Stetson were included on all four capture experiments so roughly double the
649 sequence data was obtained for this variety (Supplementary Table 1). Sequencing with
650 2x150bp reads was performed at the Earlham Institute on a NovaSeq 6000 instrument
651 (Illumina) with 16 promoter capture libraries on one lane and 16 genic capture libraries on
652 another lane.
653
654 *Variant Calls and Imputation*
655 All reads were aligned to the bread wheat reference genome from cv. Chinese Spring (RefSeq
656 v1.0)[27] using bwa-mem (version 0.7.12)[64] and sorted using samtools (version 1.3.1)[65],
657 which was also used to calculate coverage. For compatibility with the bam file format, we split
658 each chromosome in the reference genome at the halfway point before alignment. We called
659 variants from the founder sequences within the high confidence gene, promoter and 5' UTR
660 regions targeted by the capture probes[21] using GATK (version 4.0.8.0)[66] HaplotypeCaller
661 and GenotypeGVCFs (options --interval-padding 100 --minimum-mapping-quality 30). We

used vcftools (version 0.1.15) to include only bi-allelic single nucleotide polymorphisms (SNPs) with average coverage depth between 5 and 60 (all per sample coverages between 2 and 120) and no missing calls. We also filtered with bcftools (version 1.2)[67] using standard quality control options --exclude 'QD<2 || FS>60.0 || MQRankSum<-12.5 || ReadPosRankSum<-8.0 || SOR>3.0 || MQ<40'. This left 1.78M SNPs, of which we only use the 1.13M sites with no heterozygous calls (--genotype ^het option) for our main analyses.

We first called genotypes in the RILs at these 1.13M SNP sites directly using GATK HaplotypeCaller in GENOTYPE-GIVEN-ALLELES mode, using the same options as above. We assessed the concordance between array genotypes and these direct calls (AD) at overlapping sites (see below). For 10 RILs, the directly called sequencing variants most closely matched genotyping array data for a different line than expected. These were excluded because the source of the discrepancy (sequence data or array data) cannot be established. The concordance between our genotyping array data and direct calls (AD) was below 95% for a further 36 RILs, which were excluded (mean AD 84.7% for removed lines), leaving 504 RILs. We estimated heterozygosity in these 504 RILs using only genotypes called from at least four reads. Of 2.6M such genotype calls, only 0.67% were called as heterozygotes.

We imputed genotypes at the 1.13M SNP sites using the alignments and STITCH software (version 1.5.7)[26]. Because alignments were to a reference genome with chromosomes split in half, we first ran STITCH with the generateInputOnly option, and then joined the input files for each chromosome half before imputation. For all runs, we used the parameters nGen=3, minRate=0.001, bqFilter=30, method='diploid-inbred' and then filtered all sites with an info score below 0.4, minor allele frequency below 2.5%, or missingness above 10%. For our main

686 analysis, we used the genotype calls in the founders as a reference panel and outputted the
687 estimated ancestry dosages of each founder at each position in each RIL using the
688 outputHaplotypeProbabilities and output_haplotype_dosages options. When using the
689 founders as a reference panel, we removed options that estimate and update the haplotypes
690 in the population (shuffleHaplotypeIterations, reference_shuffleHaplotypeIterations,
691 refillIterations). To test accuracy when reference panels aren't available, we re-ran
692 imputation without the founder haplotypes, using 40 iterations to estimate the haplotype
693 space and recombination mosaics. We also used the downsampleFraction option to randomly
694 sample a fraction of alignments with/without using the founder reference panel. Finally, we
695 tested imputation accuracy (without a reference panel), when fewer than sixteen haplotypes
696 were assumed to segregate in the population by varying the K parameter (Supplementary
697 Figure 2).
698
699 *Genotype Comparisons*
700 For comparison against the sequencing dataset, we used all genotyping array markers.
701 Replicates of founders and MAGIC RILs (where available) were used to make a consensus call
702 where the most common genotype across replicates was taken as the consensus and only
703 retained when more than 50% of the non-missing calls were in agreement. In addition,
704 markers where one homozygous genotype was missing from all RILs were converted such that
705 all heterozygous calls were assumed to be in the missing homozygous class. The failure to
706 detect a homozygous class is likely to be a result of polyploidy, which can reduce
707 differentiation between the three genotype classes and make them hard to distinguish.
708 Finally, to get plausible physical positions for the genotyped markers, BLASTn v2.2.30[25] was
709 used to compare the 75bp probe sequences (cerealsdb.uk.net)[12] against the reference

genome[27]. When matching the SNP array data with the sequenced SNPs, array sites were excluded if there had missing or heterozygous founder calls or if the genotypes and targeted SNP alleles did not match the founder sequence data. We found 5,877 sites that overlapped between the genotyping array data and the sequencing data (Supplementary Table 2).

To compare against global wheat diversity, we called founder genotypes at 113,457 genotyping array sites that were polymorphic among 4,506 diverse global wheat accessions[13]. We called genotypes from alignments with mapping quality scores of at least 30 using GATK HaplotypeCaller in EMIT_ALL_SITES mode with the –emit-ref-confidence BP_RESOLUTION option, providing a bed file of the 113,139 genotyping array sites[13]. We only considered sites where genotypes could be called in all 16 founders (n=56,063). We used genotyping array calls for cv. Chinese Spring to determine reference/non-reference alleles on the genotyping array, ignoring sites called as heterozygous (n=109) or missing (n=306) in Chinese Spring. Seven of the MAGIC founders were also present in the global genotype set (Brigadier, Copain, Maris Fundin, Soissons, Spark, Steadfast, Stetson)[7]. The average concordance of the global genotype calls and our sequencing calls for these founders was 94.3% (sd 0.63%). We excluded 5,491 (9.8%) sites that had mismatches across these founders, many of which are likely to reflect differences in the underlying genetic variation picked up by the different genotyping technologies. Two other founder variety names were in the genotyping array dataset[7] (Banco and Holdfast) but the genotyping calls did not match (concordances 74.2% and 71.4%, respectively), which may reflect differences in the seed stock used.

732

733 ### *Founder Haplotype Diversity*

734 First, we used the SNPs called within each promoter-gene pair to estimate haplotypic diversity
735 of the founders. We calculated absolute (Manhattan) pairwise genetic distances between
736 founders at each site and then used complete linkage clustering to define haplotypic groups
737 using dist and hclust functions implemented in R statistical software (version 3.6.0)[68]. This
738 was repeated using different similarity thresholds to define haplotypes. Second, we
739 determined haplotype breakpoints using a dynamic programming algorithm. For each
740 pairwise founder combination, our algorithm calculates a mosaic of genotypic
741 similarity/dissimilarity akin to the Viterbi path from a hidden Markov model. Genotype
742 matches and mismatches are allocated a score (1 by default). To prevent excessive switching
743 between states, there is also a 'transition penalty' for inferring a change between matching
744 and mismatching states. Based on their pairwise matching/mismatching states, we then infer
745 the total number of haplotypes inferred at each site. We repeat this procedure with different
746 parameter choices (Supplementary Figure 2).

747

748 ### *Genetic Mapping and Heritability*

749 For mapping, we used the full set of 1,065,185 high-quality SNP sites called in 504 RILs after
750 imputation and quality control filters. We also selected a subset of 55,067 SNPs such that
751 every other SNP was tagged at R^2>0.99 by a member of the subset using PLINK (version 1.90)
752 with option --indep-pairwise 500 10 0.99. These tagging SNPs were used to calculate the
753 genetic relationship matrix $\boldsymbol{K} = \boldsymbol{G}\boldsymbol{G}'/p$. The phenotypic variance-covariance matrix for a
754 given vector y of standardised phenotype values was modelled as $\boldsymbol{V} = \boldsymbol{K}\sigma_g^2 + \boldsymbol{I}\sigma_e^2$ where

σ_g^2, σ_e^2 are the additive genetic and environmental variance components, estimated by maximum-likelihood[69]. The heritability of a trait was defined as $h^2 = \sigma_g^2/(\sigma_g^2 + \sigma_e^2)$. The matrix square root of the variance matrix was calculated by eigendecomposition of $\boldsymbol{V}$ as $\boldsymbol{A^2} = \boldsymbol{V}$, and the mixed model transformation of the data performed i.e. $\boldsymbol{y} \rightarrow \boldsymbol{A^{-1}y}, \boldsymbol{G} \rightarrow \boldsymbol{A^{-1}G}, \boldsymbol{V} \rightarrow \boldsymbol{I}$ to remove the inflationary effects of unequal relatedness on genetic associations before association mapping.

We performed association tests at the level of both SNPs and founder haplotypes using R statistical software (version 3.6.0)[68]. Initially, we tested the null hypothesis of no association at each SNP site in the tagging set (~55k sites). We then determined genome-wide thresholds for statistical significance using 1,000 permutations on the transformed phenotypes. If any association exceeded the 0.05 threshold (smaller p value than found across at least 950 phenotypic permutations), then we repeated the association test at all of the ~1.1M SNPs on the chromosome with the strongest association signal (lowest p value). Mapping intervals were defined to include SNPs surrounding the peak SNP, with $\log_{10}$(p) values within d units of x using $d = \max\{2, 0.1x\}$ where x is the peak $\log_{10}$(p) value. The interval for haplotype-based tests includes the range of sites that have $\log_{10}$(p) values within d units of x. SNP-based intervals were calculated using the same measure but then extended by the minimum of 5Mb or the distance to the next SNP in either direction that the same 'strain distribution pattern'[54] as any highly-associated SNPs (SNPs with $\log_{10}$(p) values within d units of x). The 'strain distribution pattern' is the pattern of major/minor alleles across founders. This procedure is designed to capture the uncertainty in the positioning of relevant recombination events either side of the QTL peak. We fitted QTLs in a stepwise manor by fitting the phenotype against the most strongly associated SNP (or haplotype

779 dosage) whenever genomewide significant QTLs were detected. The above association test
780 procedure was then repeated using the phenotype residuals after fitting all previously
781 identified QTLs. This allows closely-linked QTLs to be detected when they have different
782 patterns of causal variants among RILs. Where QTL associations were found for different
783 genotypes, they were judged to be at the same locus if they had overlapping mapping
784 intervals and at least one matching strain distribution pattern at highly-associated SNP sites.
785

786 ## *Genomic Prediction*

787 To evaluate the accuracy of trait prediction within our magic population and estimate the
788 extent of polygenic variation beyond genomewide significant QTLs, we conducted genomic
789 prediction across all phenotypes using three shrinkage-based methods: ridge regression (RR),
790 Elastic Nets (EN) and least absolute shrinkage and selection operator (LASSO). We note that
791 with appropriate choice of ridge parameter $\lambda = \sigma_e^2/\sigma_g^2$, RR is equivalent to a mixed model in
792 the sense that the RR estimated SNP effects are identical to the mixed-model Best Linear
793 Unbiased Predictors (BLUPs)[70,71]. This explains the linear correlation between estimates of
794 heritability and RR prediction accuracy (Figure 5c). For each method, we conducted 50 rounds
795 of cross validation by randomly sampling 90% of the RILs (n=454) as a training set in each
796 round to train the model, which was then used to predict the remaining 10% of RILs (n=50) -
797 the test set. For the three methods, the model equation can be written generally as $y = \mu +$
798 $\beta G + \varepsilon$, where y is the estimated trait value, μ is the model intercept, β is the vector of SNP
799 effects, G is the genotype dosage matrix, and ε is the residual error.
800

801 The genomic prediction models were trained using the R package glmnet[72], which
802 estimates an optimal lambda shrinkage value for all three genomic prediction methods based

on the training set. We then predicted phenotypes in the test set by multiplying all SNP coefficients estimates by their corresponding genotypes in the test set (and adding the intercept term). We report the training and test set prediction accuracy as the mean Pearson correlation coefficient of the predicted trait values and the actual phenotype values over 50 rounds of cross validation.

We used these genomic prediction models to simulate the potential for phenotypic change. First, we permuted the population founder haplotypes identities 40 times across 504 RILs and then projected the permuted founder genotypes onto the new lines. This creates new genetic combinations while retaining the genetic map and linkage found in the real population. We then used the three models trained as described above to predict phenotypes for the simulated MAGIC RILs. We further calculated the theoretical maximum and minimum phenotype values that are possible given the genomic prediction models and the variants segregating in the population. To estimate the maximum and minimum potentially achievable phenotype values, we trained new genomic prediction models using the full data set of 504 RILs for all phenotypes. We then calculated the maximum/minimum predicted phenotypes by summing the estimated effects for all positive/negative SNP coefficients.

Gene Deletion Analysis

We examined the power of gene-level coverage variation among founders to explain phenotypic variation. In each founder f and at each gene feature g, we computed a deletion index D_{gf}based on the number of reads aligning to the associated capture sequences, normalised by the overall coverage for that founder. The gene deletion score (GDS) for each MAGIC RIL i and feature j was computed as $S_{ij} = \sum_f H_{ijf} D_{jf}$, where H_{ijf} is the haplotype

827 dosage for founder f in RIL i at gene j, as computed by STITCH. For each phenotype a mixed-
828 model GWAS was performed, using the GDS in place of SNP dosages and with a genetic
829 relationship matrix computed from the GDS (Supplementary Table 8). We also repeated the
830 genomic prediction analysis described above by replacing the SNP genotype dosage matrix
831 with the GDS matrix (Supplementary Figure 5).
832
833 ### *Introgressions*
834 The presence of introgressions were determined using summary statistics (coverage, non-
835 reference allele frequency in founders and RILs) calculated in 10Mb windows moved in 5Mb
836 steps. Within introgressions, carriers have a high proportion of non-reference alleles due to
837 the alignment of inter-specific genetic material to the bread wheat reference genome. The
838 introgression extent was determined as the extent of 10Mb windows where all introgression
839 carriers had a higher proportion of non-reference alleles than all non-carriers. Within these
840 regions, we then checked the relative coverage of carriers and the extent to which the alleles
841 of carriers are over- or under-represented among the RILs. This evidence is summarised in
842 Supplementary Table 3. For example, the founder Maris Fundin carries a large introgression
843 (640Mb) from *Triticum timopheevi* on chromosome 2B that inflates the total number of SNPs
844 called on chromosome 2B, relative to the other chromosomes (Supplementary Figure 1), this
845 introgression is substantially over-represented among RILs, as expected[34].
846

847 Acknowledgements

848 The initiation of the NIAB DIVERSE MAGIC (NDV) population was funded by Biotechnology
849 and Biological Sciences Research Council (BBSRC) grant BB/E007201/1, awarded to IM.

Completion of the population, and its phenotypic and genetic analysis was funded by grants BB/M011666/1 to JC and BB/M011585/1 to RM, with some interim NDV germplasm development advancement supported by grant BB/I002561/1. Genomic prediction analyses were supported by grant BB/P024726/1 to RM. The small-plant phenotyping at IBERS was funded by BB/M011666/1 with additional support from BBSRC National Capability Grant BB/CAP1730/1. We thank Ana Sanchez and the temporary staff at NIAB who contributed to phenotypic data collection, and the NIAB Trials Team for management of field trial sites.

Author Contributions

Project conception and funding: IM, PH (BB/E007201/1) and RM, JC (BB/M011666/1, BB/M011585/1). Project management: JC, RM, with input from MS, NF, PH, KG and AB. Population design IM, PH. Population creation: RH, NF. Seed preparation for trials, phenotyping, trials analysis and DNA extraction: NF. Small plant phenotyping: FC. Promoter-gene capture pull downs and library preparation: TB. Genetic analyses: MS with support from RM. Genomic prediction: OL. Manuscript writing: MS, OL, NF, RM, with inputs from KG, IM and JC. All authors edited and approved the manuscript.

Availability of data and materials

The sequence datasets supporting the conclusions of this article are available in the ENA repository, under project number PRJEB39021 (temporarily embargoed), https://ebi.ac.uk/ena .

The Genotyping array genotypes for founders and MAGIC RILs are available from http://mtweb.cs.ucl.ac.uk/mus/www/MAGICdiverse/index.html in text tabular format.

The Imputed SNP genotypes and founder haplotype dosages are available from mtweb.cs.ucl.ac.uk/mus/www/MAGICdiverse/MAGIC_diverse_FILES/MAGIC_PLINK.tar.gz, and mtweb.cs.ucl.ac.uk/mus/www/MAGICdiverse/MAGIC_diverse_FILES/MAGIC_HAPLOHAPLO.tar.gz (temporary links).

The remaining datasets supporting the conclusions of this article are included within the article and its additional files.

Custom analysis scripts (mixed model and haplotype dynamic programming algorithm) are available from github.com/michaelfscott/DIVERSE_MAGIC_WHEAT .

References

1. FAO. Crop harvested area (yield and production). Crop Harvest. area (yield Prod. GAEZ. 2014.

2. Tester M, Langridge P. Breeding technologies to increase crop production in a changing world. Science (80-). 2010;327:818–22.

3. Brancourt-Hulmel M, Doussinault G, Lecomte C, Bérard P, Le Buenec B, Trottet M. Genetic Improvement of Agronomic Traits of Winter Wheat Cultivars Released in France from 1946 to 1992. Crop Sci. 2003;43:37–45.

4. Shearman VJ, Sylvester-Bradley R, Scott RK, Foulkes MJ. Physiological processes

895 associated with wheat yield progress in the UK. Crop Sci. 2005;45:175–85.

896 5. Sanchez-Garcia M, Royo C, Aparicio N, Martín-Sánchez JA, Álvaro F. Genetic improvement

897 of bread wheat yield and associated traits in Spain during the 20th century. J Agric Sci.

898 2013;151:105–18.

899 6. Mackay I, Horwell A, Garner J, White J, McKee J, Philpott H. Reanalyses of the historical

900 series of UK variety trials to quantify the contributions of genetic and environmental factors

901 to trends and variability in yield over time. Theor Appl Genet. 2011;122:225–38.

902 7. IWGSC. Shifting the limits in wheat research and breeding using a fully annotated

903 reference genome. Science [Internet]. 2018;361:eaar7191. Available from:

904 http://science.sciencemag.org/content/361/6403/eaar7191

905 8. Adamski NM, Borrill P, Brinton J, Harrington SA, Marchal C, Bentley AR, et al. A roadmap

906 for gene functional characterisation in crops with large genomes: Lessons from polyploid

907 wheat. Elife. 2020;9:1–30.

908 9. Cheng H, Liu J, Wen J, Nie X, Xu L, Chen N, et al. Frequent intra- and inter-species

909 introgression shapes the landscape of genetic variation in bread wheat. Genome Biol.

910 Genome Biology; 2019;20:1–16.

911 10. He F, Pasam R, Shi F, Kant S, Keeble-Gagnere G, Kay P, et al. Exome sequencing

912 highlights the role of wild-relative introgression in shaping the adaptive landscape of the

913 wheat genome. Nat Genet [Internet]. Springer US; 2019;51:896–904. Available from:

914 http://dx.doi.org/10.1038/s41588-019-0382-2

915 11. Juliana P, Poland J, Huerta-Espino J, Shrestha S, Crossa J, Crespo-Herrera L, et al.

916 Improving grain yield, stress resilience and quality of bread wheat using large-scale

917 genomics. Nat Genet [Internet]. Springer US; 2019;51:1530–9. Available from:

918 http://dx.doi.org/10.1038/s41588-019-0496-6

919 12. Winfield MO, Allen AM, Burridge AJ, Barker GLA, Benbow HR, Wilkinson PA, et al. High-
920 density SNP genotyping array for hexaploid wheat and its secondary and tertiary gene pool.
921 Plant Biotechnol J. 2016;14:1195–206.
922 13. Balfourier F, Bouchet S, Robert S, DeOliveira R, Rimbert H, Kitt J, et al. Worldwide
923 phylogeography and history of wheat genetic diversity. Sci Adv. 2019;5.
924 14. Hufford MB, Berny Mier Y Teran JC, Gepts P. Crop Biodiversity: An Unfinished Magnum
925 Opus of Nature. Annu Rev Plant Biol. 2019;70:727–51.
926 15. Voss-Fels KP, Stahl A, Wittkop B, Lichthardt C, Nagler S, Rose T, et al. Breeding improves
927 wheat productivity under contrasting agrochemical input levels. Nat Plants [Internet].
928 Springer US; 2019;5:706–14. Available from: http://dx.doi.org/10.1038/s41477-019-0445-5
929 16. Huang BE, Verbyla KL, Verbyla AP, Raghavan C, Singh VK, Gaur P, et al. MAGIC
930 populations in crops: current status and future prospects. Theor Appl Genet. 2015;128:999–
931 1017.
932 17. Cavanagh C, Morell M, Mackay I, Powell W. From mutations to MAGIC: resources for
933 gene discovery, validation and delivery in crop plants. Curr Opin Plant Biol. 2008/02/26.
934 2008;11:215–21.
935 18. Scott MF, Ladejobi O, Amer S, Bentley AR, Biernaskie J, Boden SA, et al. Multi-parent
936 populations in crops: a toolbox integrating genomics and genetic mapping with breeding.
937 Heredity (Edinb). Heredity (Edinb); 2020;
938 19. Ladejobi O, Elderfield J, Gardner KA, Gaynor RC, Hickey J, Hibberd JM, et al. Maximizing
939 the potential of multi-parental crop populations. Appl Transl genomics. Appl Transl Genom;
940 2016;11:9–17.
941 20. White J, Law JR, MacKay I, Chalmers KJ, Smith JSC, Kilian A, et al. The genetic diversity of
942 UK, US and Australian cultivars of Triticum aestivum measured by DArT markers and

943 considered by genome. Theor Appl Genet. 2008;116:439–53.

944 21. Gardiner LJ, Brabbs T, Akhunov A, Jordan K, Budak H, Richmond T, et al. Integrating

945 genomic resources to present full gene and putative promoter capture probe sets for bread

946 wheat. Gigascience. Oxford University Press; 2019;8:1–13.

947 22. IWGSC. A chromosome-based draft sequence of the hexaploid bread wheat (Triticum

948 aestivum) genome Ancient hybridizations among the ancestral genomes of bread wheat

949 Genome interplay in the grain transcriptome of hexaploid bread wheat Structural and

950 functional pa. Science [Internet]. 2014;345:1250092. Available from:

951 http://www.sciencemag.org/content/345/6194/1250092.abstract

952 23. Kover PXPX, Valdar W, Trakalo J, Scarcelli N, Ehrenreich IMIMM, Purugganan MDMDD,

953 et al. A Multiparent Advanced Generation Inter-Cross to fine-map quantitative traits in

954 Arabidopsis thaliana. Plos Genet. 2009/07/14. 2009;5:e1000551.

955 24. Gan X, Stegle O, Behr J, Steffen JGG, Drewe P, Hildebrand KLL, et al. Multiple reference

956 genomes and transcriptomes for Arabidopsis thaliana. Nature. 2011/08/30. 2011;477:419–

957 23.

958 25. Camacho C, Coulouris G, Avagyan V, Ma N, Papadopoulos J, Bealer K, et al. BLAST+:

959 Architecture and applications. BMC Bioinformatics. 2009;10:1–9.

960 26. Davies RW, Flint J, Myers S, Mott R. Rapid genotype imputation from sequence without

961 reference panels. Nat Genet. 2016;48:965–9.

962 27. IWGSC. Shifting the limits in wheat research and breeding using a fully annotated

963 reference genome. Science. 2018;361:eaar7191.

964 28. Cavanagh CR, Chao S, Wang S, Huang BE, Stephen S, Kiani S, et al. Genome-wide

965 comparative diversity uncovers multiple targets of selection for improvement in hexaploid

966 wheat landraces and cultivars. Proc Natl Acad Sci U S A. Proc Natl Acad Sci U S A;

967 2013;110:8057–62.

968 29. Broman KW. The genomes of recombinant inbred lines. Genetics. 2005;169:1133–46.

969 30. Pont C, Leroy T, Seidel M, Tondelli A, Duchemin W, Armisen D, et al. Tracing the ancestry

970 of modern bread wheats. Nat Genet [Internet]. Springer US; 2019;51:905–11. Available

971 from: http://dx.doi.org/10.1038/s41588-019-0393-z

972 31. Rhoné B, Raquin AL, Goldringer I. Strong linkage disequilibrium near the selected Yr17

973 resistance gene in a wheat experimental population. Theor Appl Genet. 2007;114:787–802.

974 32. Martynov SP, Dobrotvorskaya T V., Krupnov VA. Analysis of the Distribution of Triticum

975 timopheevii Zhuk. Genetic Material in Common Wheat Varieties (Triticum aestivum L.). Russ

976 J Genet. 2018;54:166–75.

977 33. Villareal RL, Toro E, Mujeeb-Kazi A, Rajaram S. The 1BL/1RS chromosome translocation

978 effect on yield characteristics in a Triticum aestivum L. cross. Plant Breed. John Wiley &

979 Sons, Ltd; 1995;114:497–500.

980 34. Tsilo TJ, Jin Y, Anderson JA. Diagnostic Microsatellite Markers for the Detection of Stem

981 Rust Resistance Gene *Sr36* in Diverse Genetic Backgrounds of Wheat. Crop Sci. John Wiley &

982 Sons, Ltd; 2008;48:253–61.

983 35. Gardner KA, Wittern LM, Mackay IJ. A highly recombined, high-density, eight-founder

984 wheat MAGIC map reveals extensive segregation distortion and genomic locations of

985 introgression segments. Plant Biotechnol J. 2016;14:1406–17.

986 36. Robert O, Abelard C, Dedryver F. Identification of molecular markers for the detection of

987 the yellow rust resistance gene Yr17 in wheat. Mol Breed. 1999;5:167–75.

988 37. Marchal C, Zhang J, Zhang P, Fenwick P, Steuernagel B, Adamski NM, et al. BED-domain-

989 containing immune receptors confer diverse resistance spectra to yellow rust. Nat Plants

990 [Internet]. Springer US; 2018;4:662–8. Available from: http://dx.doi.org/10.1038/s41477-

991 018-0236-4

992 38. Xu D, Wen W, Fu L, Li F, Li J, Xie L, et al. Genetic dissection of a major QTL for kernel

993 weight spanning the Rht-B1 locus in bread wheat. Theor Appl Genet [Internet]. Springer

994 Berlin Heidelberg; 2019;132:3191–200. Available from: https://doi.org/10.1007/s00122-

995 019-03418-w

996 39. Zhang M, Gao M, Zheng H, Yuan Y, Zhou X, Guo Y, et al. QTL mapping for nitrogen use

997 efficiency and agronomic traits at the seedling and maturity stages in wheat. Mol Breed.

998 Molecular Breeding; 2019;39.

999 40. Kuzay S, Xu Y, Zhang J, Katz A, Pearce S, Su Z, et al. Identification of a candidate gene for

1000 a QTL for spikelet number per spike on wheat chromosome arm 7AL by high-resolution

1001 genetic mapping. Theor Appl Genet [Internet]. Springer Berlin Heidelberg; 2019;132:2689–

1002 705. Available from: https://doi.org/10.1007/s00122-019-03382-5

1003 41. Wang D, Yu K, Jin D, Sun L, Chu J, Wu W, et al. Natural variations in the promoter of Awn

1004 Length Inhibitor 1 (ALI-1) are associated with awn elongation and grain length in common

1005 wheat. Plant J. 2020;101:1075–90.

1006 42. Lin M, Zhang D, Liu S, Zhang G, Yu J, Fritz AK, et al. Genome-wide association analysis on

1007 pre-harvest sprouting resistance and grain color in U.S. winter wheat. BMC Genomics

1008 [Internet]. BMC Genomics; 2016;17. Available from: http://dx.doi.org/10.1186/s12864-016-

1009 3148-6

1010 43. Beales J, Turner A, Griffiths S, Snape JW, Laurie DA. A pseudo-response regulator is

1011 misexpressed in the photoperiod insensitive Ppd-D1a mutant of wheat (Triticum aestivum

1012 L.). Theor Appl Genet. Theor Appl Genet; 2007;115:721–33.

1013 44. Kamran A, Iqbal M, Spaner D. Flowering time in wheat (Triticum aestivum L.): A key

1014 factor for global adaptability. Euphytica. 2014;197:1–26.

1015 45. Hedden P. The genes of the Green Revolution. Trends Genet. 2003;19:5–9.

1016 46. de Los Campos G, Hickey JM, Pong-Wong R, Daetwyler HD, Calus MPL. Whole-genome

1017 regression and prediction methods applied to plant and animal breeding. Genetics.

1018 Genetics; 2013;193:327–45.

1019 47. Michel S, Löschenberger F, Ametz C, Pachler B, Sparry E, Bürstmayr H. Combining grain

1020 yield, protein content and protein quality by multi-trait genomic selection in bread wheat.

1021 Theor Appl Genet [Internet]. Springer Berlin Heidelberg; 2019;132:2767–80. Available from:

1022 https://doi.org/10.1007/s00122-019-03386-1

1023 48. Michel S, Löschenberger F, Ametz C, Pachler B, Sparry E, Bürstmayr H. Simultaneous

1024 selection for grain yield and protein content in genomics-assisted wheat breeding. Theor

1025 Appl Genet [Internet]. Springer Berlin Heidelberg; 2019;132:1745–60. Available from:

1026 https://doi.org/10.1007/s00122-019-03312-5

1027 49. Gan X, Stegle O, Behr J, Steffen JGJGG, Drewe P, Hildebrand KLLKL, et al. Multiple

1028 reference genomes and transcriptomes for Arabidopsis thaliana. Nature. 2011/08/30.

1029 2011;477:419–23.

1030 50. Borrill P, Harrington SA, Uauy C. Applying the latest advances in genomics and

1031 phenomics for trait discovery in polyploid wheat. Plant J. 2019;97:56–72.

1032 51. Fradgley N, Gardner KA, Cockram J, Elderfield J, Hickey JM, Howell P, et al. A large-scale

1033 pedigree resource of wheat reveals evidence for adaptation and selection by breeders. PLoS

1034 Biol. 2019;17:1–20.

1035 52. van de Wouw M, van Hintum T, Kik C, van Treuren R, Visser B. Genetic diversity trends in

1036 twentieth century crop cultivars: A meta analysis. Theor Appl Genet. 2010;120:1241–52.

1037 53. Fu YB. Understanding crop genetic diversity under modern plant breeding. Theor Appl

1038 Genet. Springer Berlin Heidelberg; 2015;128:2131–42.

1039 54. Baud A, Hermsen R, Guryev V, Stridh P, Graham D, McBride MWMW, et al. Combined
1040 sequence-based and genetic mapping analysis of complex traits in outbred rats. Nat Genet.
1041 2013;45:767–75.
1042 55. Bogard M, Allard V, Brancourt-Hulmel M, Heumez E, Machet J-M, Jeuffroy M-H, et al.
1043 Deviation from the grain protein concentration–grain yield negative relationship is highly
1044 correlated to post-anthesis N uptake in winter wheat. J Exp Bot. Oxford Academic;
1045 2010;61:4303–12.
1046 56. Cormier F, Faure S, Dubreuil P, Heumez E, Beauchêne K, Lafarge S, et al. A multi-
1047 environmental study of recent breeding progress on nitrogen use efficiency in wheat
1048 (Triticum aestivum L.). Theor Appl Genet. 2013;126:3035–48.
1049 57. Lenz PRN, Beaulieu J, Mansfield SD, Clément S, Desponts M, Bousquet J. Factors
1050 affecting the accuracy of genomic selection for growth and wood quality traits in an
1051 advanced-breeding population of black spruce (Picea mariana). BMC Genomics. BMC
1052 Genomics; 2017;18:1–17.
1053 58. Moser G, Khatkar MS, Hayes BJ, Raadsma HW. Accuracy of direct genomic values in
1054 Holstein bulls and cows using subsets of SNP markers. Genet Sel Evol. 2010;42:1–15.
1055 59. Duncan L, Shen H, Gelaye B, Meijsen J, Ressler K, Feldman M, et al. Analysis of polygenic
1056 risk score usage and performance in diverse human populations. Nat Commun. Nature
1057 Publishing Group; 2019;10:3328.
1058 60. Liu K, Muse S V. PowerMaker: An integrated analysis environment for genetic maker
1059 analysis. Bioinformatics. 2005;21:2128–9.
1060 61. Porras-Hurtado L, Ruiz Y, Santos C, Phillips C, Carracedo Á, Lareu M V. An overview of
1061 STRUCTURE: Applications, parameter settings, and supporting software. Front Genet.
1062 2013;4:1–13.

1063 62. Mackay IJ, Bansept-Basler P, Bentley AR, Cockram J, Gosman N, Greenland AJ, et al. An
1064 eight-parent multiparent advanced generation inter-cross population for winter-sown
1065 wheat: Creation, properties, and validation. G3 Genes, Genomes, Genet. 2014;4:1603–10.
1066 63. Butler D, Cullis B, Gilmour A, Gogel B. ASReml–R Reference Manual [Internet]. Brisbane:
1067 The State of Queensland, Department of Primary Industries and Fisheries; 2009. Available
1068 from:
1069 http://scholar.google.com/scholar?hl=en&btnG=Search&q=intitle:mixed+models+for+S+lan
1070 guage+environments+ASReml-R+reference+manual#0
1071 64. Li H, Durbin R. Fast and accurate short read alignment with Burrows-Wheeler transform.
1072 Bioinformatics. 2009/05/20. 2009;25:1754–60.
1073 65. Li H, Handsaker B, Wysoker A, Fennell T, Ruan J, Homer N, et al. The Sequence
1074 Alignment/Map format and SAMtools. Bioinformatics. 2009/06/10. 2009;25:2078–9.
1075 66. McKenna A, Hanna M, Banks E, Sivachenko A, Cibulskis K, Kernytsky A, et al. The
1076 Genome Analysis Toolkit: a MapReduce framework for analyzing next-generation DNA
1077 sequencing data. Genome Res. 2010;20:1297–303.
1078 67. Li H. A statistical framework for SNP calling, mutation discovery, association mapping
1079 and population genetical parameter estimation from sequencing data. Bioinformatics.
1080 2011;27:2987–93.
1081 68. R Core Team. R: A Language and Environment for Statistical Computing. Vienna, Austria;
1082 2016.
1083 69. Kang HM, Zaitlen NA, Wade CM, Kirby A, Heckerman D, Daly MJ, et al. Efficient control
1084 of population structure in model organism association mapping. Genetics. 2008/04/04.
1085 2008;178:1709–23.
1086 70. VanRaden P. Efficient estimation of breeding values from dense genomic data. J Dairy

1087 Sci. 2007;90:374–5.

1088 71. Habier D, Fernando RL, Dekkers JCM. The impact of genetic relationship information on

1089 genome-assisted breeding values. Genetics. 2007;177:2389–97.

1090 72. Friedman J, Hastie T, Tibshirani R. glmnet: Lasso and elastic-net regularized generalized

1091 linear models. R Packag version 14. 2009;

1092